



HAL
open science

Influence of bottom roughness and ambient pressure conditions on the emplacement of experimental dam-break granular flows

Santiago Montserrat, Lady Ordoñez, Aldo Tamburrino, Olivier Roche

► **To cite this version:**

Santiago Montserrat, Lady Ordoñez, Aldo Tamburrino, Olivier Roche. Influence of bottom roughness and ambient pressure conditions on the emplacement of experimental dam-break granular flows. *Granular Matter*, 2021, 23 (3), 10.1007/s10035-021-01125-2 . hal-03254037

HAL Id: hal-03254037

<https://uca.hal.science/hal-03254037>

Submitted on 16 Jun 2021

HAL is a multi-disciplinary open access archive for the deposit and dissemination of scientific research documents, whether they are published or not. The documents may come from teaching and research institutions in France or abroad, or from public or private research centers.

L'archive ouverte pluridisciplinaire **HAL**, est destinée au dépôt et à la diffusion de documents scientifiques de niveau recherche, publiés ou non, émanant des établissements d'enseignement et de recherche français ou étrangers, des laboratoires publics ou privés.



Distributed under a Creative Commons Attribution 4.0 International License

1 **Influence of bottom roughness and ambient pressure**
2 **conditions on the emplacement of experimental**
3 **dam-break granular flows**

4 **Santiago Montserrat · Lady Ordoñez ·**
5 **Aldo Tamburrino · Olivier Roche.**

6
7 Received: DD Month YEAR / Accepted: DD Month YEAR

8 **Abstract** Geophysical granular flows occur at the surface of the Earth and
9 other planets with reduced atmospheric pressure. In this paper, we investigate
10 the run-out of dam-break flows of particle-air mixtures with fine ($d = 75\mu m$)
11 or coarse ($d = 150\mu m$) grains in a flume with different bottom roughness (δ)
12 and vacuum degrees (P^*). Our results reveal an increase of the flow run-out
13 as d/δ decreases for fine $d = 75\mu m$ -particles, and run-out decreases with the
14 dimensionless ambient pressure (P^*) for a given d/δ . In contrast, the run-out

S. Montserrat
Advanced Mining Technology Center-AMTC, Universidad de Chile, Av. Tupper 2007,
8370451, Santiago, Chile
Tel.: +56-2-29771010
E-mail: santiago.montserrat@amtc.cl

L. Ordoñez
Advanced Mining Technology Center-AMTC, Universidad de Chile, Av. Tupper 2007,
8370451, Santiago, Chile
Departamento de Ingeniería Civil, Universidad de Chile, Av. Blanco Encalada 2002, 8370449,
Santiago, Chile
Tel.: +56-2-29784400
E-mail: lady_ordonez@hotmail.es

A. Tamburrino
Departamento de Ingeniería Civil, Universidad de Chile, Av. Blanco Encalada 2002, 8370449,
Santiago, Chile
Advanced Mining Technology Center-AMTC, Universidad de Chile, Av. Tupper 2007,
8370451, Santiago, Chile
Tel.: +56-2-29784400
E-mail: atamburr@ing.uchile.cl

O. Roche
Laboratoire Magmas et Volcans, Université Blaise Pascal-CNRS-IRD, OPGC Campus
Universitaire des Cézeaux, 6 Avenue Blaise Pascal, TSA 60026 - CS 60026, 63178
AUBIERE, Cedex, France
Tel.: +33-4-73346768
E-mail: olivier.roche@uca.fr

15 for coarser $d = 150\mu m$ -particles, is almost invariant respect to P^* and d/δ .
 16 These results show that autofluidization of fine-grained flows demonstrated
 17 by earlier works at ambient pressure also occurs at reduced pressure though
 18 being less efficient. Hence, autofluidization is a mechanism, among others, to
 19 explain long run-out of geophysical flows in different environments.

20 **Keywords** Dam-break · Granular flows · Pore pressure · Ambient pressure ·
 21 Fluidization · Substrate roughness

22 1 Introduction

23 The run-out distance of dense geophysical granular flows is commonly larger
 24 than expected because the apparent friction angle is significantly reduced with
 25 respect to the repose angle of same geological materials Legros (2002); Iver-
 26 son (1997); Delannay et al. (2017). Friction reduction mechanisms have been
 27 attributed for instance to the formation of a low density bottom layer, caused
 28 by grains interacting with the bottom Cleary and Campbell (1993); Bartelt
 29 et al. (2006); Brodu et al. (2015), and/or to particle-fluid interactions caus-
 30 ing fluidization Iverson (1997); Roche et al. (2008). However, long run-outs
 31 have been observed for flows at the surface of the Earth and celestial bodies
 32 with different gravity, substrate roughness and atmospheric conditions, the lat-
 33 ter including the ambient atmospheric pressure, density and viscosity Legros
 34 (2002); Lajeunesse et al. (2006); Lucas and Mangeney (2007); Singer et al.
 35 (2012); Lucas et al. (2014). However, based on the analysis of Martian flows
 36 deposits, Lucas et al. Lucas and Mangeney (2007) show that flow run-out is
 37 independent of gravity.

38 It is argued that friction reduction can arise because moving grains inter-
 39 act with the substrate, increasing random grain-velocity fluctuations at the
 40 base of the granular flow. Thus, the bulk dense flow slides over a highly ag-
 41 itated and low concentrated basal layer reducing the apparent basal friction
 42 Campbell (1989); Cleary and Campbell (1993); Iverson (1997); Bartelt et al.
 43 (2006); Brodu et al. (2015). Recent numerical experiments shows that the
 44 basal agitated layer can reach a height of some particles diameters and has
 45 a volume concentration as low as 0.2 Brodu et al. (2015). However, friction
 46 reduction through this mechanism seems to occurs only for high speed flows on
 47 relatively steep substrates and bounded by lateral walls on which significant
 48 friction occurs.

49 Goujon et al. Goujon et al. (2003) showed experimentally that for flows of
 50 relatively large particles of size $d > 150\mu m$ and propagating on an inclined
 51 rough plane, the main parameter controlling flow friction was the ratio be-
 52 tween the size of the flowing particles (d) and the size of roughness (δ). They
 53 found that flow friction was maximum at $d/\delta \sim 0.5$. They also argued that the
 54 increase in the flow run-out for $d/\delta < \sim 0.5$ was probably because the particles
 55 filled the substrate interstices, thus reducing the effective roughness. However,
 56 changes in flow run-out with d/δ was almost negligible for slope angles lower

57 than $\sim 18^\circ$. The negligible dependence of the flow run-out with d/δ on hori-
58 zontal planes was confirmed by experiments of Lube et al. (2004)
59 for $d > 300\mu m$ and maximum values of $d/\delta \sim 1$.

60 The presence of an interstitial fluid can be a key factor for friction reduction
61 in granular flows, especially those containing high amounts of fine particles
62 ($\sim 100\mu m$) that confer low hydraulic permeabilities Iverson (1997); Iverson
63 and Denlinger (2001); Roche et al. (2010); Montserrat et al. (2012, 2016);
64 Chédeville and Roche (2018); Breard et al. (2018). Excess pore fluid pressure,
65 naturally arising from upwards fluid fluxes and/or particle settling, reduces
66 interparticle friction by locally decreasing contact forces Iverson (1997); Iver-
67 son and Denlinger (2001); McArdell et al. (2007); Montserrat et al. (2012).
68 Excess pore fluid pressure, high above hydrostatic levels, was measured both
69 in laboratory experiments and in natural flows in the field Iverson (1997); Iver-
70 son et al. (2010); Roche et al. (2010); McArdell et al. (2007). Chédeville and
71 Roche Chedeville and Roche (2014); Chédeville and Roche (2015) found that
72 flows of fine particles on a rough substrate experienced autofluidization. This
73 occurred as the flow particles settled into the interstices of the substrate and
74 forced the air to escape upwards and to percolate through the flow. Autoflu-
75 idization thus increased the flow run-out compared to a smooth substrate, and
76 this effect was enhanced as the substrate roughness increased because more air
77 was available for autofluidization. On the same principle, autofluidization occurs
78 also in collapsing beds of fine particles released from some height above a solid
79 surface, as demonstrated by numerical simulations Breard et al. (2018) and
80 laboratory experiments Chédeville and Roche (2018). Fine-grained mixtures
81 can also be fluidized through mechanical vibrations that cause fluid-particle
82 relative oscillations and related high pore fluid pressure, a phenomenon called
83 acoustic streaming Valverde and Soria-Hoyo (2015); Soria-Hoyo et al. (2019).

84 Fluidization of granular flows rich in fine particles, however, is uncertain in
85 case the atmospheric pressure is significantly lower than on Earth, as it is the
86 case on Mars for instance (4×10^{-3} to 9×10^{-3} bar). Therefore, we experimen-
87 tally explore the effect of the ambient air pressure and substrate roughness on
88 the run-out of granular flows. We perform dam-break type experiments involv-
89 ing different particle sizes, substrate roughness, and degrees of vacuum. To this
90 end, we constructed a sealed channel that allowed us to make experiments up
91 to $\sim 99\%$ of vacuum relative to the ambient atmosphere. To our knowledge,
92 this is the first investigation conducted under vacuum conditions and using
93 fine particles. Previous granular flow experiments under high vacuum condi-
94 tions were performed with coarser particles and showed no significant effects
95 of the vacuum degree on flow emplacement Börzsönyi and Ecke (2006). Our
96 results highlight the importance of the ambient fluid and bottom roughness
97 in increasing flow-run out of fine particles ($d \sim 75\mu m$) even at low vacuum
98 degrees, while for coarser particles ($d \geq 150\mu m$) both effects are negligible.

99 2 Materials and Methods

100 We conducted dam-break experiments in a sealed lock-exchange channel 180
 101 cm-long, 19.3 cm-wide and 50 cm-high (Figure 1). A sluice gate separates the
 102 channel from the reservoir at the upper end, where the particles are retained.
 103 This section is 100 cm high, so that the gate can be opened inside the device.
 104 The reservoir has a length $x_o = 20\text{cm}$. We generate granular flows by a rapid
 105 vertical release of the sluice gate ($< 0.1\text{s}$). The experimental device is made
 106 of a 30 mm-thick transparent plexiglass to permit flow visualization and to
 107 resist high degrees of vacuum. It is also equipped with a vacuum pump to
 108 reduce ambient air pressure, and the degree of vacuum is measured using a
 109 *EdwardsAPG100 – XM* vacuummeter. The maximum degree of vacuum that
 110 can be reached in the channel system is of the order of $\sim 1\%$ of the atmo-
 111 spheric pressure. For the range of ambient pressures we use (1% to 100% of
 112 the atmospheric pressure), air viscosity remains constant Börzsönyi and Ecke
 113 (2006); Bello (2017).

114 The bottom of the channel is covered by a 10 mm-thick aluminum sheet
 115 over which the granular flow propagates. Different roughnesses were obtained
 116 by gluing a single layer of particles of diameter δ to the aluminum base. We
 117 tested three different bottom roughness conditions: i) aluminum roughness,
 118 ii) $\delta = 1\text{mm}$ roughness and iii) $\delta = 3\text{mm}$ roughness. Onward, the smooth
 119 aluminum roughness condition will be denoted as $\delta = 0$.

120 We used two different types of near spherical glass beads (Ballotini, Potters
 121 Industries) with characteristics diameters $d_1 \sim 75\mu\text{m}$ ($\sim 40\mu\text{m}$ to $\sim 140\mu\text{m}$)
 122 and $d_2 \sim 150\mu\text{m}$ ($\sim 70\mu\text{m}$ to $\sim 300\mu\text{m}$), repose angles $\theta_1 = 27.1^\circ \pm 0.4^\circ$
 123 and $\theta_2 = 27.7^\circ \pm 0.3^\circ$, and both with a particle density of $\rho_p = 2500\text{kg/m}^3$.
 124 Particles were carefully poured inside the reservoir in order to achieve near
 125 constant mixture densities, $\rho_1 = 1360 \pm 15\text{kg/m}^3$ for $d \sim 75\mu\text{m}$ -particles and
 126 $\rho_2 = 1412 \pm 6\text{kg/m}^3$ for $d \sim 150\mu\text{m}$ -particles, resulting in initial particle

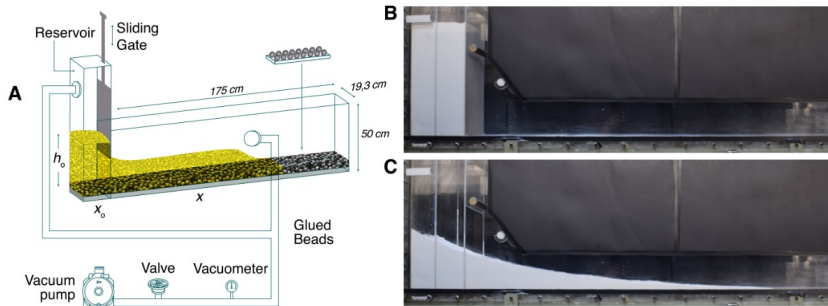


Fig. 1 A) Sketch of the experimental device. h_o and x_o denotes the initial height and length of the column of particles inside the reservoir, respectively, while x is the flow-front position measured from the gate, B) Side view of the experimental channel before removing the gate. Particles (in white) are in the reservoir. C) Side view of the final deposit

127 volume concentrations $c_{v1} = 0.54 \pm 0.01$ and $c_{v2} = 0.56 \pm 0.01$ (i.e. particle-
 128 mixture porosity $\phi_1 = 0.46 \pm 0.01$ and $\phi_2 = 0.44 \pm 0.01$). Particles bed heights
 129 in the reservoir where varied from $h_o \sim 20cm$ to $h_o \sim 40cm$ (in terms of mass,
 130 from $\sim 10.5kg$ to $\sim 22.5kg$).

131 In our experiments, and due to the relatively narrow grain size range of
 132 the materials, we did not expect significant particle size segregation in the
 133 reservoir, flow or deposit. Thus, segregation was neglected in our analysis. In
 134 addition, the channel width to particle size ratio was of the order of ~ 2550
 135 and ~ 1280 for fine and coarse particles respectively, so that negligible sidewall
 136 effects were expected. However, side wall effects seem to be responsible in
 137 reducing flow run out in case of initial high column aspect ratios ($h_o/x_o > 1.5$)
 138 respect to low column aspect ratios Roche et al. (2011); Montserrat et al.
 139 (2016). Nevertheless, these differences are less than the observed experimental
 140 variability and we assumed that sidewall effects had a negligible influence on
 141 our flows.

142 3 Results

143 3.1 Flow run-out distance

144 The run-out distance of flows of particles of size $d = 75\mu m$ shows an important
 145 increase with both ambient pressure and substrate roughness. Figure 2 shows
 146 that, for these particles, the dimensionless flow run-out ($x_f^* = x_f/h_0$) increases
 147 fairly linearly with the dimensionless ambient pressure $P^* = P_o/P_{atm}$ (where
 148 P_o denotes for the ambient pressure inside the channel and P_{atm} is the at-
 149 mospheric pressure in the laboratory). The dimensionless flow run-out under
 150 vacuum conditions (i.e. $P^* = 0$), inferred from the best linear fits shown in
 151 Figure 2, increases from $x_f^* = 2.3$ to $x_f^* = 3.5$, and $x_f^* = 3.8$ for smooth, 1 mm
 152 and 3 mm-substrate roughnesses, respectively. This corresponds to a flow run-
 153 out increase of 52 % and 65 %, for 1 mm and 3 mm roughnesses, respectively,
 154 compared to the smooth case in the absence of an interstitial fluid. In addition,
 155 the substrate roughness increases the growth rate of the dimensionless
 156 flow run-out with the ambient pressure. While the slope of the fitted straight
 157 lines for the case of the smooth surface is 0.79, it increases to 1.75 and 2.29
 158 for 1 mm and 3 mm-substrate roughnesses, respectively. This results in values
 159 of $x_f^* = 3.1$, $x_f^* = 5.2$ and $x_f^* = 6.1$ for smooth, 1 mm and 3mm-substrate
 160 roughnesses, respectively, at laboratory ambient conditions ($P^* = 1$). This
 161 corresponds to an increase of the flow run-out of 68% and 97% for 1 mm and
 162 3 mm-roughnesses, respectively, compared to the smooth case.

163 The flow run-out distance for particles of size $d = 150\mu m$ shows to be
 164 independent of both the ambient pressure and surface roughness (Figure 2),
 165 except for the case of $\delta = 3mm$, where a slight increasing tendency of the
 166 flow run-out is observed with P^* . The dimensionless run-out for $d = 150\mu m$
 167 particles is always significantly lower than that of flows of $d = 75\mu m$ particles
 168 for the same range of ambient pressure and channel roughness. Note that at

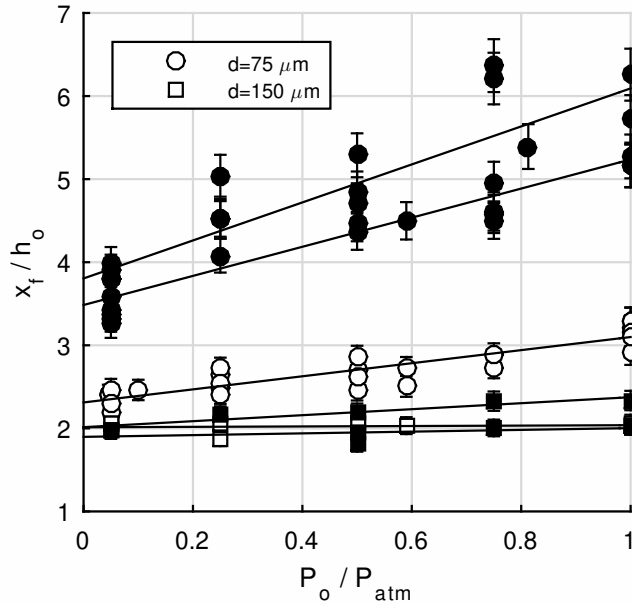


Fig. 2 Dimensionless flow run-out, x_f/h_o , as a function of the dimensionless ambient pressure P_o/P_{atm} (with P_o the ambient pressure inside the channel and P_{atm} the atmospheric pressure in the laboratory). White, gray and dark symbols represent smooth, 1 mm and 3 mm bottom roughness respectively. Note that symbols may be larger than error bars.

169 vacuum conditions, the dimensionless flow run-out for $d = 75\mu m$ ($x_f^* = 2.3$)
 170 on a smooth substrate is slightly higher ($\sim 15\%$) than that for $d = 150\mu m$
 171 ($x_f^* = 2$).

172 3.2 Flow-front dynamics and flow morphology of fine particle mixtures

173 In this section, we examine fine particles mixtures as no significant changes in
 174 the flow front dynamics and flow morphology are observed for coarser particles
 175 ($d \sim 150\mu m$), neither with P^* nor δ . In addition, and to simplify the analysis,
 176 we only compare the obtained results between the two roughness extremes
 177 used in the experiments (i.e. $\delta = 0$ and $\delta = 3mm$).

178 Figure 3 shows the dimensionless flow front position, $x^* = x/h_o$, for
 179 $d = 75\mu m$ -particles, as a function of the dimensionless time, $t^* = t/(h_o/g)^{1/2}$
 180 Roche et al. (2008), where x denotes the horizontal flow front position mea-
 181 sured from the gate, t is time, and g is the gravitational acceleration, for dif-
 182 ferent vacuum conditions and for a smooth substrate ($\delta = 0$). The flow front
 183 propagates in three different phases, as known for flows under atmospheric
 184 pressure conditions Lajeunesse et al. (2005); Roche et al. (2008); Xu et al.
 185 (2016); Lube et al. (2005). Under atmospheric conditions ($P^* = 1$), Figure
 186 3 shows a first phase for which the flow front accelerates (first phase) until
 187 it reaches a constant front velocity U equal to $\alpha(gh_o)^{1/2}$, where α is a pro-

188 proportionality constant close to ~ 1 Roche et al. (2008). The constant velocity
 189 phase occurs for $\sim 1.5 < t^* < \sim 3.0$. A second transition occurs at $t^* \sim 3.0$,
 190 where the flow starts decelerating until it comes to halt at $t^* \sim 5 - 5.5$.

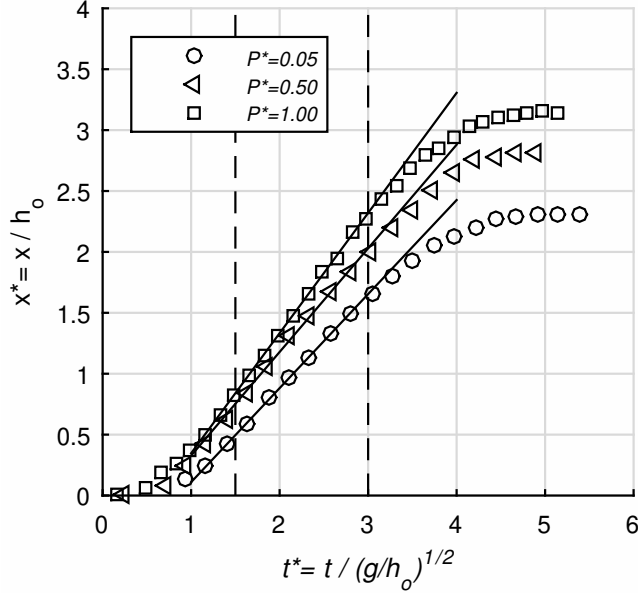


Fig. 3 Dimensionless flow front position x^* for different values of P^* and $\delta = 0$

191 The same trend is observed at reduced atmospheric conditions (Figure 3),
 192 with the transitions between phases occurring at the same values of t^* than
 193 for laboratory ambient pressure (i.e. $P^* = 1$). The main effect of the ambient
 194 pressure is a velocity decrease in the constant-velocity phase, with α decreasing
 195 from $\alpha = 0.99$ at laboratory atmospheric conditions to $\alpha = 0.85$ and $\alpha = 0.77$
 196 at $P^* = 0.50$ and $P^* = 0.05$, respectively.

197 Figure 4 shows that the front position for fine particles flows ($d = 75\mu m$)
 198 at $\delta = 0$ and $\delta = 3mm$ and different vacuum degrees are almost identical
 199 until $t^* \sim 3.0$. However, for rough substrates ($\delta = 3mm$), the constant veloc-
 200 ity phase lasts longer. For example, for $\delta = 3mm$, the transition between the
 201 second and third phase occurs at $t^* \sim 5$. In addition, increasing roughness sig-
 202 nificantly reduces the front deceleration, thus increasing the flow run-out and
 203 duration Chedeville and Roche (2014); Chédeville and Roche (2015). While
 204 flows on a smooth substrate stop at $t^* \sim 5 - 5.5$, almost independently of P^* ,
 205 at $\delta = 3mm$ flow duration last up to $t^* \sim 7$, $t^* \sim 8$ and $t^* \sim 9$ for $P^* = 0.05$,
 206 $P^* = 0.50$ and $P^* = 1.00$, respectively.

207 These kinematics can be complemented considering the flow morphology,
 208 which varies very little with the channel roughness until the end of the constant
 209 velocity phase for smooth surfaces ($t^* \sim 3$), regardless of P^* (Figure 5). For
 210 $t^* > 3$, the flow length increases with the substrate roughness and this is

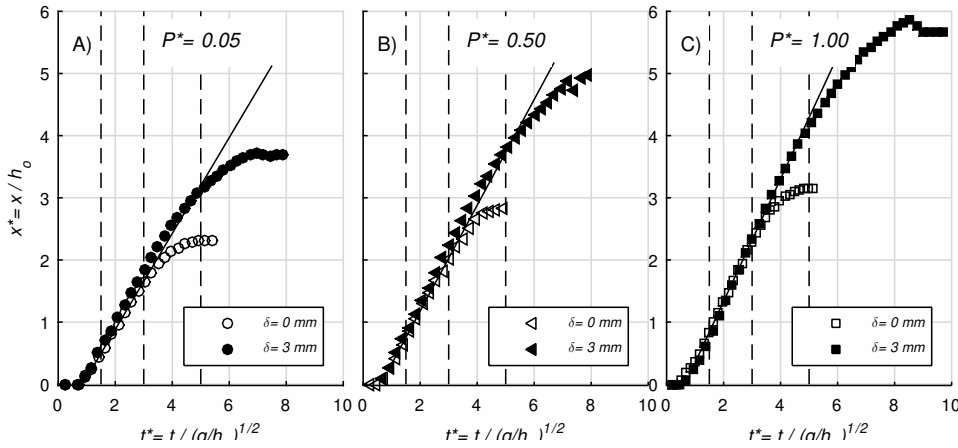


Fig. 4 Dimensionless flow front position, x^* , for different values of P^* and δ , for fine $75\mu\text{m}$ particles

211 mainly because a thin flow head arises from the flow body, even after the latter
 212 has stopped Chedeville and Roche (2014). Slight differences in the position of
 213 the center of area (equivalent to the center of mass in 3D) of the flow for
 214 smooth and 3 mm rough surfaces confirm that the increasing flow length with
 215 roughness is due to the very thin frontal part of the flow that propagates
 216 downstream and causes long run-out.

217 4 Discussion

218 Sustained high pore fluid pressure has been pointed out as one of the primary
 219 friction reduction mechanisms in experimental flows of initially fluidized fine
 220 ($< \sim 100\mu\text{m}$) granular materials propagating on smooth or rough surfaces at
 221 earth atmospheric conditions Roche et al. (2008, 2010); Montserrat et al. (2012,
 222 2016); Chedeville and Roche (2014); Chédeville and Roche (2015); Breard et al.
 223 (2018); Chédeville and Roche (2018). Notice that initially non-fluidized flows
 224 with shorter run-out distances have the ability to self-generate excess pore
 225 fluid pressure to near $\sim 15\%$ of the weight of the particle, possibly because of
 226 granular mixture compaction Roche et al. (2010) or by air incorporation at the
 227 flow front Bareschino et al. (2008). However, this last mechanism has shown
 228 to be negligible in experimental flows Chédeville and Roche (2015). Recent
 229 dam-break experiments show that the mixture porosity is correlated with flow
 230 velocity as it decreases during flow acceleration (i.e. mixture dilation) and
 231 increases during flow deceleration (i.e. mixture compaction) Xu et al. (2016).
 232 In case of granular compaction, pore pressure rises by the compression of air
 233 trapped in the interstices if the time scale for particles rearrangement (T_R) is
 234 small compared with the time scale for vertical pore pressure diffusion (T_D)
 235 Homan et al. (2014). The opposite occurred in case of mixture dilation (i.e.
 236 pore pressure drops when the mixture and pores dilate). For a given change in

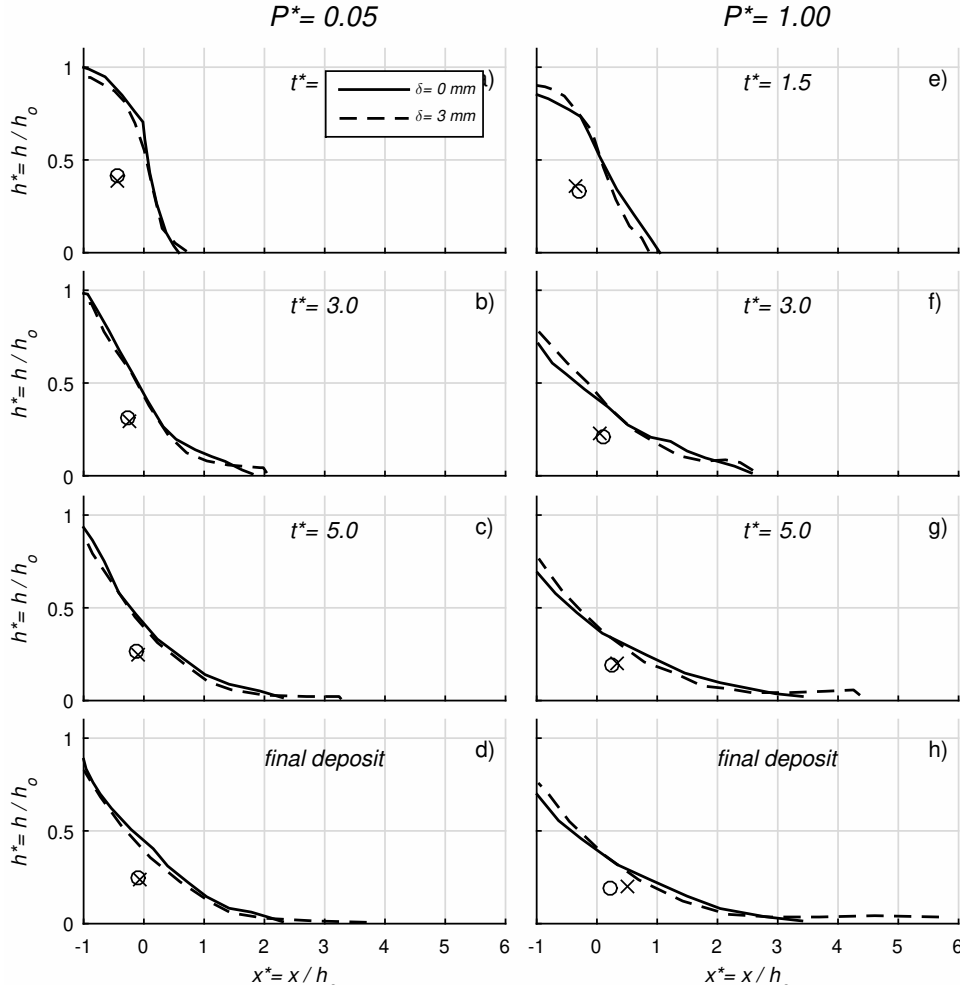


Fig. 5 Flow morphology for different δ and P^* . \circ and \times denotes for the center of area of the flowing mixture for $\delta = 0$ and $\delta = 3\text{mm}$, respectively.

237 air volume (ΔV_a), and assuming isothermal air compression, the upper limit
 238 for pore pressure variations (ΔP) respect to the ambient pressure (P_o) can be
 239 approximated as Homan et al. (2014):

$$\Delta P = -P_o \frac{\Delta V_a}{V_a} \quad (1)$$

240 where V_a is the volume of air in the interstices and ΔV_a is defined positive for
 241 air dilation and negative for air compression. In equation (1), non linear terms
 242 have been neglected Homan et al. (2014).

243 As $P_o = P^* P_{atm}$, equation (1) shows that for similar changes in the air
 244 volume between grains, $|\Delta P|$ linearly decreases with the degree of vacuum

($\Delta P \sim P^*$). Thus, autofluidization is possible even under reduced atmospheric conditions, and decreasing the ambient pressure will linearly decrease the amount of pore pressure changes. This can explain the observed linear trends between the flow run-out and the degree of vacuum ($x_f/h_o \sim P^*$, see Figure 2), at least for the case $\delta = 0$ and $d = 75\mu m$ -particles. In this sense, reducing P_o increases the effective flow friction, which also agrees with the observed reductions in flow duration and flow-front velocities during the constant velocity phase.

For flows over rough substrates ($\delta = 1\text{ mm}$ and $\delta = 3\text{ mm}$), fluidization can arise because of particles falling into the substrate interstices and forcing the air to percolate upwards through the granular flow Chedeville and Roche (2014); Chédeville and Roche (2015). The amount of pore fluid pressure due to drag interactions (Δp) increases with air velocity and can be accounted in packed beds by the semi-empirical Ergun equation Gibilaro (2001), here expressed in terms of the degree of fluidization ($\Delta p^* = \Delta p/P_L$) of a granular column of height h and bulk density ρ :

$$\Delta p^* = \frac{\Delta p}{P_L} = 150 \frac{\mu_g U_g}{\rho g d^2} \frac{(1 - \phi)^2}{\phi^3} + 1.75 \frac{\rho_g U_g^2}{\rho g d} \frac{1 - \phi}{\phi^3} \quad (2)$$

where μ_g is the gas dynamic viscosity, U_g is the superficial gas velocity (defined as the flow rate per unit cross sectional area), ρ_g is the gas density and ϕ is the particle-mixture porosity (defined previously). We assumed that changes of porosity was negligible during flow emplacement, making the Ergun equation relevant for describing fluidization. The first and second terms at the right-hand of equation 2 accounts for viscous and inertial fluidization, respectively.

$\Delta p^* = 1$ means that the entire weight of the particle bed is supported by air drag, which occurs at a minimum value of U_g called the minimum fluidization velocity, U_{mf} . Solving equation 2 for $\Delta p^* = 1$ results in $U_{mf} = 11\text{ mm/s}$ and $U_{mf} = 32\text{ mm/s}$ for $d = 75\mu m$ and $d = 150\mu m$ -particles, respectively. These values scale with previous experimental measurements done on similar materials Roche et al. (2004). Chédeville and Roche Chedeville and Roche (2014) estimate that particles falling into the interstices generate upward air fluxes above U_{mf} -values due to the high settling velocities of the particles. For the estimated values of U_{mf} , the first term on the right hand side of equation 2 is ~ 1 , while the second term is $\sim 10^{-3}$, meaning that fluidization is mainly due to viscous drag. Thus, for the range of P -values used for this experiments, for which μ is constant, autofluidization related to a rough substrate is always possible, even at high vacuum conditions. This explains the increasing run-out of $d = 75\mu m$ -particles mixtures compared to a smooth substrate even at very low ambient pressure conditions ($P^* \sim 0.05$). U_{mf} for $d = 150\mu m$ -particles is larger than for $d = 75\mu m$ -particles. As both types of particles fall into the interstices as about the same velocity, then the interstitial air velocity should be in the same order in both cases. However, this result in smaller Δp^* for $d = 150\mu m$ -particle mixtures, explaining the almost null effect of P^* in the run-out of these flows. The slight increase of x_f^* with P^* observed for $\delta = 3\text{ mm}$, suggests that higher volumes of air trapped into the interstices

288 are able to sustain vertical air fluxes for longer periods, promoting a weak
 289 fluidization compared with $d = 75\mu\text{m}$ -particles flows.

290 An alternative (or complementary) friction reduction mechanism, consist-
 291 ing in the development of a low density layer at the flow bottom because
 292 of flow particles colliding with those of the bottom roughness, may also be
 293 considered. In this context, the flow run-out is expected to be a function of
 294 d/δ Goujon et al. (2003). In the case of a smooth surface (aluminum sub-
 295 strate) we assume $d/\delta = 1$, as it has been observed that the flow rides over a
 296 thin layer of the same particles deposited after the passage of the flow-front
 297 Lube et al. (2004). Thus, for $d = 75\mu\text{m}$ -particles $d/\delta = 1 - 0.025$, while for
 298 $d = 150\mu\text{m}$ -particles $d/\delta = 1 - 0.05$. Although d/δ varies in a similar range
 299 for both types of particles, the flow run-out with d/δ for $d = 150\mu\text{m}$ -particles
 300 does not vary significantly. This suggests that viscous fluidization controls the
 301 flow mechanism of fine granular mixtures and confirms that, in the absence of
 302 autofluidization, d/δ does not control the flow run-out in horizontal channels.

303 5 Conclusions

304 Our results confirm that viscous air-particle interactions are an important fric-
 305 tion reduction mechanism for fine-grained granular flows. In our experiments,
 306 the relative increase of flow run-out with the substrate roughness is reduced as
 307 the ambient pressure decreases, but such increase is still significant (65%, from
 308 $\delta = 0$ to 3 mm) even at $P^* = 0.05$ (Figure 2). This suggests that the autoflu-
 309 idization mechanism acting in flows of fine particles on rough substrate and
 310 at atmospheric pressure Chedeville and Roche (2014); Chédeville and Roche
 311 (2015) operates as well at lower pressures. This can be explained because vis-
 312 cosity remains constant for the range of vacuum conditions explored in this
 313 study and because, for particles of this size range, fluidization is dominated
 314 by fluid viscosity Bello (2017); Roche et al. (2008).

315 The above-mentioned friction reduction mechanisms does not act for coarser
 316 particle materials ($d \sim 150\mu\text{m}$). This can be explained as the air initially
 317 present in the substrate interstices is expelled upwards at lower velocities
 318 compared with the minimum fluidization velocity (U_{mf}) of the coarse par-
 319 ticles (see Chédeville and Roche Chedeville and Roche (2014) for experiments
 320 at $P^* = 1$) or because the amount of air trapped in the interstices is not
 321 enough to fluidize the particle mixture over a significant duration. An excep-
 322 tion occurs for $\delta = 3\text{ mm}$, where a slight influence of P^* in the flow run-out is
 323 observed. In addition, for coarser $d \sim 150\mu\text{m}$ -particles, the increasing rough-
 324 ness does not have significant effects on the flow run-out, even for a similar
 325 range of d/δ compared with $d = 75\mu\text{m}$ -particles flows. Thus, in the absence of
 326 fluidization capacity of the flowing mixture, increasing roughness shows not to
 327 be an important friction reduction mechanism in granular flows. However, this
 328 mechanism could become important for high-velocity flows on steep substrates
 329 Brodu et al. (2015).

330 Regarding the motion of the flow front of fine-grained mixtures, decreasing
331 the ambient pressure mainly results in a decrease in velocity and duration of
332 the constant velocity phase. This is a consequence of the reduction of the aut-
333 offluidization capacity, proportional to $|\Delta P|$, which causes increasing friction.
334 Increasing δ increases the flow run-out by increasing the time of the constant
335 velocity phase and the stopping phase. This is because, for larger δ , the air is
336 expelled from the substrate for longer duration as more air is trapped initially
337 in their interstices. However, the increase in flow run-out is due to a thin flow-
338 ing frontal layer that spreads from the flow body at $t^* \sim 3$, which represents a
339 little amount of the total mass. Thus, the run-out of the bulk flow, represented
340 by the run-out of the center of area of the avalanche (see Figure 5), is almost
341 independent of d/δ .

342 Our findings have implications for granular mass flows on extraterrestrial
343 planets with reduced atmospheric pressure. They suggest that fluidization
344 caused by viscous drag may occur through vertical gas fluxes within the gran-
345 ular flow, even at low ambient pressure. This is likely to occur when flows
346 propagating on rough substrates contain high amounts of fine particles that
347 settle into the substrate interstices. However, fluidization may also arise from
348 air compression (i.e. increasing pore pressure) during fast contraction of the
349 particle network. This second mechanism decreases when reducing the atmo-
350 spheric pressure, thus increasing flow friction and reducing the flow run-out.
351 This is likely to be important for fine particle flows, where the time for particle
352 rearrangements is small compared with the time for pore pressure diffusion

353 **Acknowledgements** This work was supported by the Advanced Mining Technology Cen-
354 ter (AMTC) and Departamento de Ingeniería Civil, from Universidad de Chile, the French
355 National Research Institute for Sustainable Development (IRD, France) and the Chilean Na-
356 tional Commission for Scientific and Technological Research, CONICYT, through Fondecyt
357 Projects 1130910 and 11130254 and PIA Project AFB180004. We thank P. Mendoza and
358 two anonymous reviewers for helpful comments on our work. We also thank C. González
359 for his assistance with graphics. This is Laboratory of Excellence ClerVolc contribution No
360 XXX.

361 **Compliance with Ethical Standards** The authors declare that they
362 have no conflicts of interest. The study was supported by the Advanced Min-
363 ing Technology Center (AMTC) from Universidad de Chile, and the Chilean
364 National Commission for Scientific and Technological Research, CONICYT,
365 through Fondecyt Projects 1130254.

366 References

- 367 Bareschino P, Lirer L, Marzocchella A, Petrosino P, Salatino P (2008)
368 Self-fluidization of subaerial rapid granular flows. *Powder Technology*
369 182(3):323–333, DOI 10.1016/j.powtec.2007.12.010
- 370 Bartelt P, Buser O, Platzer K (2006) Fluctuation dissipation relations for
371 granular snow avalanches. *Journal of Glaciology* 52(179):631–643, DOI
372 10.3189/172756506781828476

- 373 Bello I (2017) Vacuum and Ultravacuum. CRC Press, DOI
374 10.1201/9781315155364
- 375 Börzsönyi T, Ecke RE (2006) Rapid granular flows on a rough incline: Phase di-
376 agram, gas transition, and effects of air drag. *Physical Review E* 74(6):61,301
- 377 Breard ECP, Dufek J, Lube G (2018) Enhanced Mobility in Con-
378 centrated Pyroclastic Density Currents: An Examination of a Self-
379 Fluidization Mechanism. *Geophysical Research Letters* 45(2):654–664, DOI
380 10.1002/2017GL075759
- 381 Brodu N, Delannay R, Valance A, Richard P (2015) New patterns in
382 high-speed granular flows. *Journal of Fluid Mechanics* 769:218–228, DOI
383 10.1017/jfm.2015.109
- 384 Campbell CS (1989) Self-lubrication for long runout landslides. *The Journal*
385 *of Geology* pp 653–665
- 386 Chédeville C, Roche O (2014) Autofluidization of pyroclastic flows prop-
387 agating on rough substrates as shown by laboratory experiments. *Journal*
388 *of Geophysical Research: Solid Earth* 119(3):1764–1776, DOI
389 10.1002/2013JB010554
- 390 Chédeville C, Roche O (2015) Influence of slope angle on pore pressure gen-
391 eration and kinematics of pyroclastic flows: insights from laboratory exper-
392 iments. *Bulletin of Volcanology* 77(11):96, DOI 10.1007/s00445-015-0981-4
- 393 Chédeville C, Roche O (2018) Autofluidization of collapsing bed of
394 fine particles: Implications for the emplacement of pyroclastic flows.
395 *Journal of Volcanology and Geothermal Research* 368:91–99, DOI
396 10.1016/j.jvolgeores.2018.11.007
- 397 Cleary PW, Campbell CS (1993) Self-lubrication for Long Runout Landslides:
398 Examination by computer simulation. *Journal of Geophysical Research:*
399 *Solid Earth* 98(B12):21,911–21,924, DOI 10.1029/93JB02380
- 400 Delannay R, Valance A, Mangeney A, Roche O, Richard P (2017) Granular
401 and particle-laden flows: from laboratory experiments to field observations.
402 *Journal of Physics D: Applied Physics* 50(5):053,001, DOI 10.1088/1361-
403 6463/50/5/053001
- 404 Gibilaro LG (2001) *Fluidization dynamics*. Elsevier
- 405 Goujon C, Thomas N, Dalloz-Dubrujeaud B (2003) Monodisperse dry granular
406 flows on inclined planes: Role of roughness. *The European Physical Journal*
407 *E* 11(2):147–157, DOI 10.1140/epje/i2003-10012-0
- 408 Homan T, Gjaltema C, van der Meer D (2014) Collapsing granular beds:
409 The role of interstitial air. *Physical Review E* 89(5):052,204, DOI
410 10.1103/PhysRevE.89.052204
- 411 Iverson RM (1997) The Physics of Debris. *Review of Geophysics* 35(97):245–
412 296, DOI 10.1029/97RG00426
- 413 Iverson RM, Denlinger RP (2001) Flow of variably fluidized granular
414 masses across three-dimensional terrain: 1. Coulomb mixture theory.
415 *Journal of Geophysical Research: Solid Earth* 106(B1):537–552, DOI
416 10.1029/2000JB900329
- 417 Iverson RM, Logan M, LaHusen RG, Berti M (2010) The perfect debris flow?
418 Aggregated results from 28 large-scale experiments. *Journal of Geophysical*

- 419 Research: Earth Surface 115(F3):n/a—n/a, DOI 10.1029/2009JF001514
- 420 Lajeunesse E, Monnier JB, Homsy GM (2005) Granular slumping on a hori-
421 zontal surface. *Physics of fluids* 17:103,302, DOI doi.org/10.1063/1.2087687
- 422 Lajeunesse E, Quantin C, Allemand P, Delacourt C (2006) New insights on the
423 runout of large landslides in the Valles-Marineris canyons, Mars. *Geophysical*
424 *Research Letters* 33(4), DOI 10.1029/2005GL025168
- 425 Legros F (2002) The mobility of long-runout landslides. *Engineering Geology*
426 63(3):301–331, DOI 10.1016/S0013-7952(01)00090-4
- 427 Lube G, Huppert HE, Sparks RSJ, Hallworth MA (2004) Axisymmetric col-
428 lapses of granular columns. *Journal of Fluid Mechanics* 508(1):175–199, DOI
429 10.1017/S0022112004009036
- 430 Lube G, Huppert HE, Sparks RSJ, Freundt A (2005) Collapses of two-
431 dimensional granular columns. *Physical Review E* 72(4):041,301, DOI
432 10.1103/PhysRevE.72.041301
- 433 Lucas A, Mangeney A (2007) Mobility and topographic effects for large Valles
434 Marineris landslides on Mars. *Geophysical research letters* 34(10):L10,201,
435 DOI 10.1029/2007GL029835
- 436 Lucas A, Mangeney A, Ampuero JP (2014) Frictional velocity-weakening in
437 landslides on Earth and on other planetary bodies. *Nature communications*
438 5, DOI 10.1038/ncomms4417
- 439 McArdell BW, Bartelt P, Kowalski J (2007) Field observations of basal forces
440 and fluid pore pressure in a debris flow. *Geophysical Research Letters* 34(7),
441 DOI 10.1029/2006GL029183
- 442 Montserrat S, Tamburrino A, Roche O, Niño Y (2012) Pore fluid pressure
443 diffusion in defluidizing granular columns. *Journal of Geophysical Research*
444 117(F2):F02,034, DOI 10.1029/2009JB007133
- 445 Montserrat S, Tamburrino A, Roche O, Niño Y, Ihle CF (2016) Enhanced run-
446 out of dam-break granular flows caused by initial fluidization and initial
447 material expansion. *Granular Matter* 18(1):1–9, DOI 10.1007/s10035-016-
448 0604-6
- 449 Roche O, Gilbertson MA, Phillips JC, Sparks RSJ (2004) Experimental study
450 of gas-fluidized granular flows with implications for pyroclastic flow em-
451 placement. *Journal of Geophysical Research: Solid Earth* 109(B10), DOI
452 10.1029/2003JB002916
- 453 Roche O, Montserrat S, Niño Y, Tamburrino A (2008) Experimental observa-
454 tions of water-like behavior of initially fluidized, dam break granular flows
455 and their relevance for the propagation of ash-rich pyroclastic flows. *Journal*
456 *of Geophysical Research* 113(B12):B12,203, DOI 10.1029/2008JB005664
- 457 Roche O, Montserrat S, Niño Y, Tamburrino A (2010) Pore fluid pressure and
458 internal kinematics of gravitational laboratory air-particle flows: insights
459 into the emplacement dynamics of pyroclastic flows. *Journal of Geophysical*
460 *Research* 115:B09,206, DOI 10.1029/2009JB007133
- 461 Roche O, Attali M, Mangeney A, Lucas A (2011) On the run-out distance
462 of geophysical gravitational flows: Insight from fluidized granular collapse
463 experiments. *Earth and Planetary Science Letters* 311(3):375–385, DOI
464 10.1016/j.epsl.2011.09.023

- 465 Singer KN, McKinnon WB, Schenk PM, Moore JM (2012) Massive ice
466 avalanches on Iapetus mobilized by friction reduction during flash heating.
467 Nature Geoscience 5(8):574–578, DOI doi.org/10.1038/ngeo1526
- 468 Soria-Hoyo C, Valverde JM, Roche O (2019) A laboratory-scale study on the
469 role of mechanical vibrations in pore pressure generation in pyroclastic ma-
470 terials: implications for pyroclastic flows. Bulletin of Volcanology 81(2):12,
471 DOI [10.1007/s00445-019-1271-3](https://doi.org/10.1007/s00445-019-1271-3)
- 472 Valverde JM, Soria-Hoyo C (2015) Vibration-induced dynamical weak-
473 ening of pyroclastic flows: Insights from rotating drum experiments.
474 Journal of Geophysical Research: Solid Earth 120(9):6182–6190, DOI
475 [10.1002/2015JB012317](https://doi.org/10.1002/2015JB012317)
- 476 Xu X, Sun Q, Jin F, Chen Y (2016) Measurements of velocity and pres-
477 sure of a collapsing granular pile. Powder Technology 303:147–155, DOI
478 [10.1016/j.powtec.2016.09.036](https://doi.org/10.1016/j.powtec.2016.09.036)